Cement and Concrete Research 40 (2010) 260–270

Contents lists available at ScienceDirect

Cement and Concrete Research

journal homepage: http://ees.elsevier.com/CEMCON/default.asp

Effect of air voids on salt scaling and internal freezing

Zhenhua Sun, George W. Scherer *

Princeton University, Civil & Env. Eng./PRISM, Eng. Quad. E-319, Princeton, NJ 08544, USA

ARTICLE INFO

Article history:
Received 21 January 2009
Accepted 29 September 2009

Keywords:
Pore size distribution (B)
Freezing and Thawing (C)
Thermal analysis (B)

ABSTRACT

By combining calorimetric measurements with dilatometry, it has been possible to calculate the contributions of thermal expansion, pore pressure, and crystallization pressure of ice to the strain observed in a mortar during freezing/thawing cycles. Air-entrained mortars contract upon freezing, while non-air-entrained mortars expand. The expansion of the latter is attributed primarily to hydraulic pressure, owing to the rapid growth of ice, which nucleates at low temperatures in laboratory samples. Poromechanical calculations account quantitatively for the contraction of samples with air entrainment, assuming that ice crystals form in the air voids. As originally proposed by Powers and Helmuth, those crystals create suction in the pore liquid that offsets the crystallization pressure of ice in the mesopores of the paste, resulting in a net contraction. Ice in the matrix also contributes significantly to the increase in the thermal expansion coefficient of the mortar.

The magnitude of the contraction in air-entrained mortar is shown to account for a reduction of salt scaling damage. According to the glue-spall theory, the damage results from cracking of the ice on the surface of concrete, when the thermal expansion mismatch stress exceeds the strength of the ice. The contraction of the mortar caused by air entrainment offsets the thermal expansion mismatch sufficiently to prevent cracking.

Based on observations of the nucleation temperature of ice in laboratory samples of various sizes, it is estimated that there is one site capable of nucleating ice at −1 °C in a cube of mortar roughly 34 cm on an edge (or, one per square meter in a slab 3 cm thick). This suggests that ice nucleates in the field at high temperatures, compared to what is typically seen in the laboratory, and propagates slowly through the pores as the temperature drops. This mode of growth may lead to fatigue damage over many cycles, owing to local stresses from crystallization pressure, where the contribution of hydraulic pressure is insignificant.

1. Introduction

Salt scaling is a type of superficial damage that occurs when the surface of concrete is exposed to ice and salt (or other solute) [1]. The phenomenology of scaling has been extensively reviewed [2–4] and a theory, called the "glue-spall" model, has been proposed that seems to account for most of the observations [5]. Briefly, the idea is that the ice layer binds mechanically to the surface of the concrete, and tensile stress develops in the ice as the temperature descends, owing to the higher thermal expansion of the ice (50×10^{-6}/°C for ice versus ~10×10^{-6}/°C for concrete). If the stress is high enough to cause the ice to crack, the crack will penetrate the surface of the concrete, then turn and remove a flake; if the ice is pure, then it is too strong to crack, and if the solute content is high, then the ice remains too soft to damage the concrete. At intermediate salt contents (~2–5 wt.%), unfrozen pockets of brine act as stress concentrators that promote cracking of the ice and consequent damage to the underlying concrete. This model explains the dependence of scaling damage on solute concentration and temperature cycle [5], and it predicts a dependence on the thickness of the ice layer that has recently been verified [6]. The principles are also supported by finite-element simulations [7]. To account for the observation [1,6] that scaling damage is strongly reduced by use of air-entraining agents (AEA), the glue-spall theory offers two suggestions: a) the AEA reduces bleeding of pore water, so the surface is stronger and more resistant to scaling [5]; b) air-entrained concrete contracts when it freezes, and this offsets the thermal expansion mismatch with ice, so cracking of the ice is reduced [4]. The purpose of the present paper is to make a quantitative assessment of the validity of the second suggestion.

Tremblay et al. [6] made a careful study of scaling using a series of mortars with a range of water/cement ratio (w/c) and amount of entrained air (0, 3, and 6 vol.%). The air content was shown to have a dramatic effect on scaling. In the present work, we have used samples of the same mortars. We measured the amount of ice formation in the mortar with a differential scanning calorimeter (DSC) and observed the dimensional changes during cooling and reheating in a differential mechanical analyzer (DMA). We will show that the observed dilatation can be quantitatively explained on the basis of poromechanics

* Corresponding author.
E-mail address: scherer@princeton.edu (G.W. Scherer).

0008-8846/$ – see front matter © 2009 Elsevier Ltd. All rights reserved.
doi:10.1016/j.cemconres.2009.09.027

[8,9], and that the contraction of air-entrained mortar is sufficient to account for the reduced salt scaling.

To perform the strain calculations, we must know the size and shape of pores that are filled with ice as a function of temperature. As we will show, the required data are most directly obtained calorimetrically. A detailed discussion of those measurements is presented elsewhere [10]; only the pertinent results are included here.

2. Experimental procedure

The samples used in the present experiments were provided by Tremblay et al. (Laval University), who prepared the samples for the work presented in Ref. [6]. All mortars were made from ASTM Type I ordinary Portland cement. A low percentage (20% by volume) of Ottawa sand type C-109 was used as fine aggregate to improve mixture homogeneity. Mixtures were prepared at two water/binder ratios (0.40 and 0.55) and three different air contents (0, 3 and 6 vol.%) using a synthetic detergent air-entraining agent (Microair by BASF). Batching was done using a counter-current pan mixer. A Welan gum-based viscosity modifying agent was added at the end of the mixing sequence to minimize internal bleeding. They were stored in a wet room at 100% RH and 23 °C from 24 h after mixing until they were sent to us (at an age of about 1.5 years); they had dried in transit, but were immersed in limewater (*i.e.*, water saturated with calcium hydroxide) in our lab until use (about 6 months).

The length change of samples during freezing was measured with a Perkin-Elmer differential mechanical analyzer (DMA7e). Samples with dimensions of about 5×5×15 mm were cut from the mortar cylinders. The samples were saturated by storage in limewater for months. When the sample freezes in the DMA, the volume change causes ice to extrude through the surface, which can displace the sensor, even if the sample does not expand. To avoid this problem, the sample was dried briefly under ambient conditions to minimize ice extrusion. During the measurement, the sample was immersed in clear odorless kerosene and the instrument was cooled down to as low as −40 °C. To encourage ice nucleation, metaldehyde (Acros) [11] was used in some cases on the surface of the samples. The as-received metaldehyde powder was lightly ground in a mortar and pestle, then sprinkled on the surface of the sample, which was then wrapped with tape to insure good contact of the powder with the mortar. One air-entrained sample (w/c = 0.55, 6% air) was immersed in water and subjected to 2.5 MPa of pressure for 12 h to fill the voids with water before freezing in the DMA.

To calculate the contraction expected from the negative pore pressure during freezing, it is necessary to know the elastic properties of the porous body. Therefore, the static elastic (Young's) modulus was measured using a strain gauge (Epsilon Extensometer) on the cylindrical mortar sample while compressing it at a crosshead speed of 1 mm/min to a maximum strain of 0.1% with an INSTRON 600 mechanical testing machine. The samples had an irregular cross-section, because pieces had been cut from the original 10×20 cm cylinders for other tests, but the loaded area could be accurately found by dividing the weight by the height and density of the sample. The dynamic modulus was also obtained from the acoustic velocity, which was measured using 54 kHz transducers (PUNDIT).

To measure the porosity of the samples, the weights of both fully saturated and dried samples were measured. The samples were vacuum saturated by placing them in a desiccator and evacuating the vessel for 3 h, and then back-filling with water for another 2 h. The fully saturated samples were weighed and then dried in the oven at 105 °C for 2 days and weighed again; the pore volume of the sample was then calculated from the weight difference of wet and dry samples, assuming that the pore water has a density of 1.0 g/cm^3. This high temperature removes interlayer water [12] and may cause some dehydration of C–S–H or ettringite [13]. Our purpose is to find the volume of pore liquid that can exert pressure on the body, and it seems reasonable to exclude the interlayer water from that quantity, as argued by Ghabezloo et al. [14]. Therefore, we also used a milder drying treatment intended to remove water only from the capillary and gel pores. Mortars were exchanged into isopropanol and weighed after drying at 60 °C; the weight gain after resaturating with water was used to determine the porosity. To determine the skeletal density, mortars with 0 and 6% entrained air were measured by helium pycnometry (Micromeritics Accupyc 1330) after exchange into isopropanol and drying at 60 °C for 2 weeks.

DSC data can be used to determine the pore size distribution, since the freezing point of the pore water is reduced by the curvature of the crystal/liquid interface, κ_{CL}, according to the Gibbs–Thomson equation:

$$\gamma_{CL}\kappa_{CL} = \int_T^{T_M(\infty)} \frac{(S_L - S_C)}{V_L} dT \tag{1}$$

where γ_{CL} is the crystal/liquid interfacial energy, S_L and S_C are the entropies of the liquid and crystal, respectively, $T_M(\infty)$ is the melting point of a macroscopic crystal, and V_L is the molar volume of the liquid. This technique, called thermoporometry (TPM), was described in detail by Brun et al. [15], who pioneered its development. Based on comparisons of MIP and TPM results for various porous materials, they concluded that an unfrozen film of water with a thickness of about $\delta \approx 0.8$ nm remained between the crystal and the pore wall. Therefore, if the pore is a cylinder with radius r, then the advancing interface is hemispherical, with $\kappa_{CL} = 2/(r-\delta)$. During freezing, the amount of heat released at temperature T indicates the volume of pores that are accessible through entries with radius r given by Eq. (1). During reheating, the curvature of the pore interior controls the melting temperature, so a hysteresis is observed that is analogous to that seen in adsorption/desorption isotherms; for a cylindrical crystal, the curvature controlling the melting temperature is $\kappa_{CL} = 1/(r-\delta)$. For the calculation of freezing strain, we only need to know the amount of ice in the pores as a function of temperature; details about the pore size and shape determined calorimetrically are presented elsewhere [10].

Bulk water can be cooled below 0 °C without freezing, owing to the energetic barrier to nucleation, and this effect must not be confused with the effect of pore size on freezing temperature. Therefore, to determine the effect of pore size on freezing temperature, it is necessary to cool the sample until some of the pore liquid freezes, then to heat to a point just below the melting point [15]. This procedure creates crystals that reside in the macropores (or on the surface of the sample), and these crystals propagate through the pores as the temperature is decreased again. During the second cooling cycle, the invasion of the crystal phase through the pores is strictly analogous to the invasion of mercury during mercury intrusion porosimetry (MIP) or of vapor during the desorption cycle in a nitrogen adsorption/desorption (NAD) experiment; however, the stress that is exerted on the porous host by the ice is about 10 times less than that exerted by mercury in a pore of the same size [16]. More importantly, the TPM sample does not have to be dried (indeed, it must be fully saturated), so the pore structure is not altered by capillary pressure. The importance of this was demonstrated by Villadsen [17], who compared the pore size distributions found from MIP, TPM, and NAD; moreover, he compared MIP samples dried following methanol exchange, and he performed TPM on samples that had been dried and resaturated. His results, some of which were presented in Ref. [18], clearly show that drying increases the pore volume and pore size compared to that of an undried sample.

To confirm the total pore volume, mortar samples were examined by TPM, MIP, and NAD. To minimize the difference in the results obtained by these methods, the samples were subjected to the same preparation procedure. The limewater-saturated paste was immersed in isopropanol for 12 h to replace the water in the pores with alcohol, then dried in an oven at 60 °C for 12 h; after that, the DSC samples were vacuum saturated, as described above for porosity measurements. To

maximize the sensitivity, samples were cut in the form of disks ~5×5×1 mm thick to fill the DSC pan. A drop of kerosene was added on top of the sample to improve thermal contact with the aluminum sample pan and to minimize drying of the sample while the lid is being crimped onto the pan. The temperature cycles ranged from +5 °C to about −40 °C at a rate of 0.25 °C/min using a Perkin-Elmer Differential Scanning Calorimeter (Pyris 1), which had been calibrated using pure water. The accuracy of the temperature measurement is ±0.1 °C and that of the enthalpy is ±2%. The interpretation of TPM data for mortar is complicated by the presence of solutes in the pore water. Since our samples were stored for an extended period in limewater, the alkali are likely to have diffused out, so the pores are expected to contain a solution very similar to limewater. Measurements on porous glass containing either pure water or limewater confirm that the solute has a negligible effect on the results [10].

The use of mercury intrusion for measuring the pore size of cementitious materials is problematic, because drying is known to alter the microstructure (*e.g.*, the permeability rises by two orders of magnitude, apparently as a result of microcracking [19]); moreover, the pressure exerted during intrusion can cause damage [20]. The samples prepared for the scaling tests had been dried in transit, so the drying damage was largely done before our tests began. However, some of that damage probably healed by hydration during lengthy storage (several months) in limewater. Before mercury intrusion porosimetry (MIP), the water-saturated samples were exchanged in isopropanol, and then dried at 60 °C. MIP measurements were performed using a Micromeritics 9410 on granules ~2 mm in diameter. One measurement was made shortly after the samples were obtained, and another about a year later (contemporaneously with the DSC measurements). As reported in the next section, a significant decrease in pore volume resulted from the year of aging in limewater, so we compare the DSC results to the later MIP data. This means that the pore structure of our samples is different from that of the younger samples used in the scaling study [6]; however, the samples measured in this study by DMA and DSC were strictly equivalent. Similar samples were characterized by nitrogen sorption using a Micromeritics ASAP 2010.

3. Results

The porosity and modulus values for the mortars are shown in Table 1. An upper bound on the porosity, ϕ, is found from the weight loss upon heating to 105 °C. Dividing the bulk density $1-\phi$ yields a skeletal density of 2430±30 kg/m^3, but this is an overestimate; the values from helium pycnometry are about 4% lower. For the sample without air entrainment, given the bulk density ($\rho_b = 1.681$ g/cm^3) and the skeletal density from pycnometry ($\rho_s = 2.318$ g/cm^3), the pore volume is $V_p = 1/\rho_b - 1/\rho_s = 0.164$ cm^3/g, and the porosity is $\phi = 1-\rho_b/\rho_s = 0.275$. The values of air content in the mortars that were measured in Ref. [6] are shown in the table, along with values estimated from the ratios of the bulk densities of the dry samples, and they are seen to be consistent. The ratios of the saturated densities show that the sample with a nominal air content of 3% has a density 2% lower than the sample without air entrainment, so the air voids are largely empty. The sample with a nominal air content of 6% has a saturated density 5.5% lower than sample without AEA, so its voids are also empty. After the non-air-entrained mortar was exchanged into alcohol and dried at 60 °C, it was resaturated with water; the weight gain corresponded to a pore volume of 0.161 ml/g, which agrees well with the value calculated from the pycnometry data.

The amount of ice formed during freezing and melting on each cycle agrees within about 6%, as shown in Table 2. This level of agreement is only obtained by taking proper account of the temperature dependence of the thermodynamic properties; in particular, if the heat of fusion is treated as a constant, the amount of ice formed on freezing appears to differ from the amount melted by almost 20%. The hysteresis in the amount of ice is large, as shown in Fig. 1 for the mortar containing 6% air.

Fig. 2 shows the strain measured in the DMA on mortar samples with nominal entrained air contents of 0, 3, and 6%. All of the samples nucleate at about −6 °C (when metaldehyde is applied), after which the air-entrained samples contract while the other sample expands. The same behavior was observed by Powers and Helmuth [21]. The role of the air voids in causing contraction is further illustrated in Fig. 3, which shows the expansion of an air-entrained sample whose pores were filled with water by application of pressure.

Table 1
Modulus and porosity of mortar with w/c = 0.55.

Air content (vol%)[a]	0 (1.5) [0]	3 (5.0) [4.0]	6 (5.8) [6.0]
Saturated density[b] (kg/m^3)	1993	1953	1884
Bulk density[c] (kg/m^3)	1681	1614	1517
Skeletal density[d] (kg/m^3)	2443 (2498) [2318]	2442 (2642)	2397 (2638) [2313]
Porosity[e]	0.312 (0.268)	0.339	0.367 (0.333)
Dynamic E (GPa)	28.5	27.7	24.9
Static E (GPa)	20.1	18.6	16.0

[a] Nominal air content (Measured value from Ref. [6]) [Calculated from ratio of dry bulk densities].
[b] Sample saturated, except for air voids.
[c] Calculated from initial volume and weight after drying at 105 °C.
[d] Calculated from bulk density and porosity (Calculated from bulk density and porosity, allowing for measured volume of air voids) [From helium pycnometry].
[e] Calculated from weight loss at 105 °C (after drying at 60 °C).

4. Discussion

4.1. Freezing in pores

From the DSC data, we can calculate the volume fraction, ϕ_C, of the pore space that freezes at a given undercooling. The result, shown in Fig. 1, is needed to calculate the dilatation of the body in Section 4.3. We can also use these data to determine the consequences of undercooling before nucleation occurs. For example, if ice first forms at -10.6 °C, as in Fig. 3, the ice can immediately invade 21% of the pore space. Since the growth rate is high at such a low temperature, the resulting hydraulic pressure is quite damaging in a mortar without air entrainment.

The static pressure in the liquid, p_L, can be found using a formula developed by Coussy and Monteiro [22],

$$p_L - p_{atm} \approx \left(\frac{V_C - V_L}{V_C}\right)\frac{\phi_C}{\phi_C/K_C + (1-\phi_C)/K_L} \tag{2}$$

where V_C and V_L are the molar volumes and K_C and K_L are the bulk moduli of the crystal and liquid, respectively. This equation is based on the assumption that the surface of the sample is sealed (or, equivalently, that the air voids are very far apart), so that the hydraulic pressure resulting from the volume change cannot escape; thus, it constitutes an upper bound on the pore pressure. For ice and water, the property values are $V_C = 19.65$ cm^3/mol [23], $V_L = 18.0$ cm^3/mol [23], $K_C = 8.8$ GPa [24], and $K_L = 2.2$ GPa [23]. At −10.6 °C, Fig. 1 indicates that $\phi_C = 0.21$, so Eq. (2) yields $p_L \approx 46$ MPa. Assuming that all pores

Table 2
Volume of ice (ml/g) detected by DSC.

Cycle	Freezing (ml/g)	Melting (ml/g)
1	0.0891	0.0943
2	0.0993	0.0936
3	0.101	0.0957

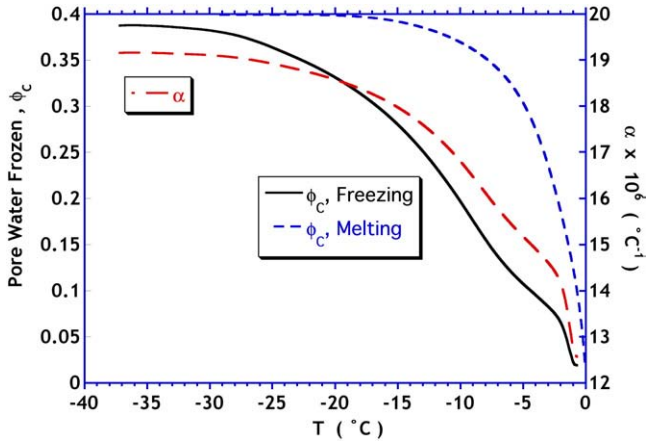

Fig. 1. Left axis: volume fraction of the pore space filled with ice, ϕ_C, versus temperature during freezing and melting cycles, from DSC data on mortar without air entrainment; pore volume 0.161 cm^3/g. Right axis: thermal expansion coefficient of mortar containing ice, α, calculated using theory from Ref. [32].

deform to the same degree when subjected to the same pressure, the linear strain of the body is given approximately by [9]:

$$\varepsilon_x \approx \left(\frac{1}{3K_p} - \frac{1}{3K_S}\right)[\phi_C p_A + (1-\phi_C)p_L] + \alpha\Delta T \tag{3}$$

where K_p and K_S are the bulk moduli of the porous body and the solid phase itself, α is the thermal expansion of the body (including contributions from mortar and ice), and p_A is the pressure applied on the pore walls by the crystals. The static Young's modulus of the mortar with 6% air is reported in Table 1 to be $E_p = 16.0$ GPa, and it is reasonable to assume that Poisson's ratio is $\nu_p \approx 0.2$, so $K_p = E_p/[3(1-2\nu_p)] \approx$ 8.9 GPa. It has been suggested [25] that the bulk modulus of the solid can be estimated from $K_p \approx K_s(1-\phi)^2$. This value is slightly lower than the lowest upper bound for a two-phase composite where one phase is void, which Hashin and Shtrikman [26] found to be:

$$K_p \approx K_S\left(\frac{1-\phi}{1+\phi}\right) \tag{4}$$

We use the latter bound, with $K_p = 8.9$ GPa and $\phi = 0.333$ to find $K_S = 17.8$ GPa. Ignoring the pressure from the crystals, Eqs. (2)

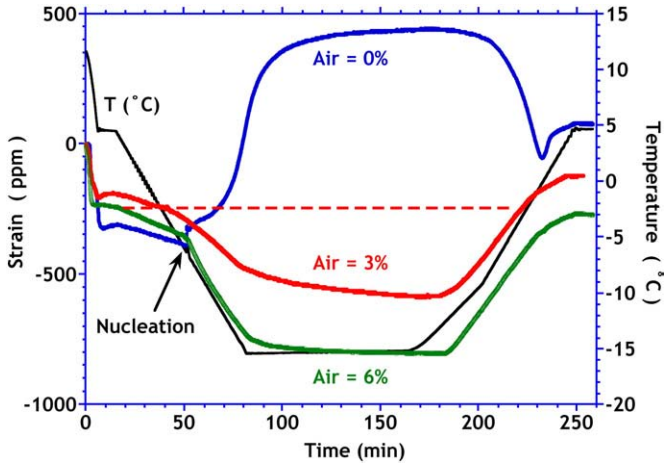

Fig. 2. Strain measured during cooling of saturated mortar in DMA, following temperature cycle shown on the right ordinate. All samples nucleated at a temperature of about −6 °C, owing to the use of a nucleating agent (metaldehyde). The air-entrained samples both contract immediately upon freezing, while the non-air-entrained sample expands.

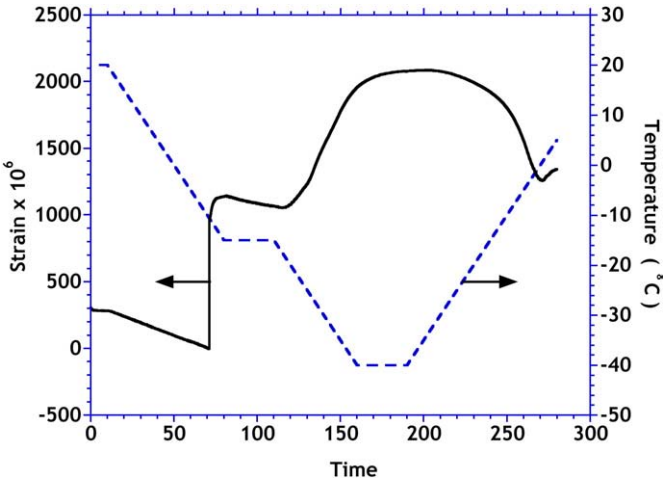

Fig. 3. Strain measured in DMA during cooling of a mortar with 6% air entrainment, but which was subjected to ~2.5 MPa pressure while submerged in water to fill the air voids. Nucleation occurred at about −10.6 °C, because no nucleating agent was used. In contrast to the air-entrained samples in Fig. 2, the pressurized sample expands on freezing, as the air voids are full of water.

and (3) indicate that the strain caused by freezing at −10.6 °C should be about 6.8×10^{-4}. This is greater than the strain limit for fracture, $\varepsilon_F \approx \sigma_T/E_p \approx 2.5\times10^{-4}$, given a maximum tensile strength of $\sigma_T \approx$ 4 MPa (estimated to be ~10% of the compressive strength, which was measured to be 39.8 MPa at 56 days [6]). Therefore, we conclude that the hydraulic pressure alone is sufficient to damage the sample without air entrainment, when ice nucleates at −10.6 °C. These are overestimates of the pressure and strain, because the high pressure in the liquid would inhibit growth of ice, according to the Clausius–Clapeyron equation, so ϕ_C would be smaller than the values given in Fig. 1, which apply when the liquid pressure is atmospheric. Nevertheless, the correction would not be large enough to change the conclusion that pore pressure is destructive, if nucleation occurs well below the melting point.

If the pore pressure were free to escape, then the strain would be given by Eq. (3) with $p_L = 0$. We will consider that case in Section 4.4. In the next section, we consider the influence of air voids on p_L.

4.2. Freezing strain

Fig. 4 shows the strain of the mortar with 6% air, replotted from Fig. 2 as a function of T. The increase in slope following nucleation is a consequence of the suction created in the mesopores by ice crystals in the air voids [11]. The situation is shown schematically in Fig. 5 (see the detailed discussion in Ref. [27][1]): the macroscopic ice crystal in the air void bulges into the mesopores surrounding the void (Fig. 5a), but does not enter them until the temperature, T, is low enough. The curvature, κ_{CL}, of the crystal/liquid interface is related to T by the Gibbs–Thomson equation, Eq. (1). If the entropy is constant, that equation reduces to:

$$T = T_M(\infty) - \frac{\gamma_{CL}\kappa_{CL}}{(S_L - S_C)/V_L} \tag{5}$$

If we assume the bulge to be a hemisphere with radius r, then $\kappa_{CL} = 2/r$, and:

$$r = 2\gamma_{CL}\Big/\int_{T_M(r)}^{T_M(\infty)} \Delta S_{fv}\,dT \approx \frac{2\gamma_{CL}}{\Delta S_{fv}[T_M(\infty) - T_M(r)]} \tag{6}$$

[1] There are two typographical errors in Ref. [27] of which we are aware: the minus sign in Eq. (13) should not be there, and the plus sign in front of the entropy term on the right side of Eq. (44) should be a minus sign.

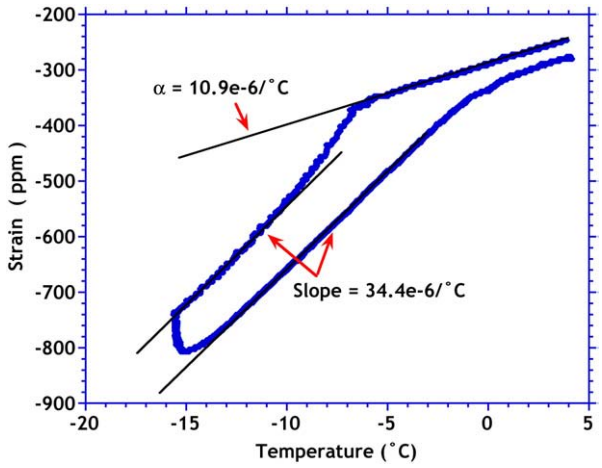

Fig. 4. Strain measured in DMA during cooling of a mortar with 6% air entrainment (data from Fig. 2). Before nucleation occurs at about −6.5 °C, the slope represents the thermal expansion coefficient of the saturated mortar, α. After freezing, the slope increases to 34.4×10^{-6} °C^{-1} as a result of the suction in the liquid caused by the ice in the air voids.

where $\Delta S_{fv}=(S_L-S_C)/V_L>0$. The ice escapes from the void and penetrates a mesopore with radius r_p when the temperature is low enough so that $r=r_p-\delta$, where δ is the thickness of the unfrozen layer of water against the pore wall (see Fig. 5b), which is 2–3 molecular layers thick (~0.8 nm for pure water [15], or ~1.0–1.2 nm in cement paste [10]). Before the ice enters the mesopores, it sucks water from those pores into the void, creating a negative pressure in the water-filled pores equal to [27]:

$$p_L-p_{atm}=-\int_{T_M(r)}^{T_M(\infty)}\Delta S_{fv}dT\approx\Delta S_{fv}[T_M(r)-T_M(\infty)] \tag{7}$$

It is this pressure that causes the contraction of the air-entrained samples after nucleation of ice. The pressure created by the meniscus in the void is sustained by water/ice or water/air menisci in other voids and at the outer surface of a concrete body. In our experiments, the sample is surrounded with kerosene, so there are water/kerosene menisci at the surface. The water/kerosene interfacial energy is about 0.042–0.047 J/m^2 [28–30], whereas the water/ice interfacial energy is about 0.04 J/m^2 [15], so we expect those external menisci to sustain the pore pressure until the ice escapes from the voids.

At the same time that ice in the air voids is creating suction, the DSC results indicate that there are ice crystals that nucleate in the mesopores and occupy volume fraction ϕ_C of the pore space. Those crystals apply a pressure p_A on the pore walls whose magnitude depends on the shape of the crystal. Suppose that a crystal of ice occupies a pore in which the radius of the pore body, r_B, is larger than that of the pore entry, r_E, as in Fig. 5c. Assuming that the curvature of the ice at the pore entry is in equilibrium with the temperature of the water, according to Eq. (6), then the pressure on the pore wall is given by Eq. (6) of Ref. [27] (see also Ref. [31]):

$$p_A=\gamma_{CL}(\kappa^E_{CL}-\kappa^S_{CL})\equiv\gamma_{CL}\kappa^E_{CL}(1-\lambda) \tag{8}$$

where κ^E_{CL} and κ^S_{CL} are the curvatures at the pore entry and pore side, respectively, and we define the pore shape parameter, λ, as:

$$\lambda\equiv\frac{\kappa^S_{CL}}{\kappa^E_{CL}}=\int_{T_M(r_B)}^{T_M(\infty)}\Delta S_{fv}dT\Big/\int_{T_M(r_E)}^{T_M(\infty)}\Delta S_{fv}dT \tag{9}$$

where $T_M(r_E)$ is the melting point of ice with a radius of curvature sufficient to enter the pore and $T_M(r_B)$ is the melting point of ice with the radius of curvature of the interior of the pore body. If the entropy

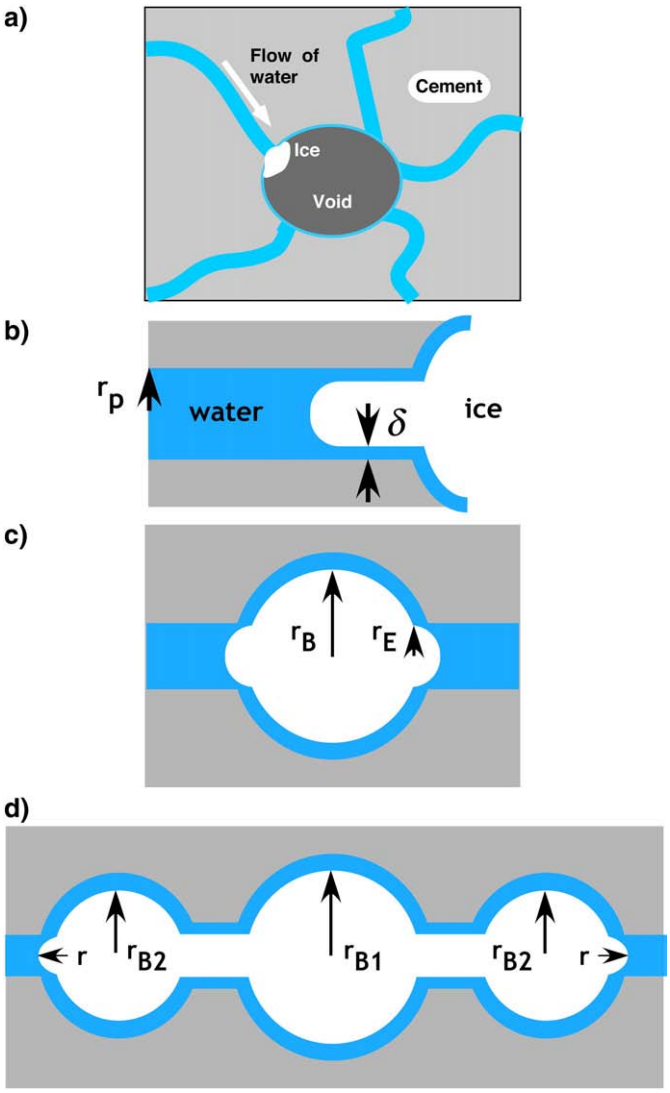

Fig. 5. a) Schematic illustration of a macroscopic ice crystal in an air void that sucks water from the surrounding mesopores (shaded channels). The curvature of the crystal/liquid interface where the ice bulges into the mesopore is related to the temperature by Eq. (6). Before the ice can penetrate into that pore, it creates a negative pressure given by Eq. (7). b) Ice penetrating a mesopore with radius r_p is separated from the pore wall by a liquid film with thickness δ. c) A crystal in a pore where the radius of the pore body, r_B, differs from that of the pore entry, r_E. d) Crystal spreading through the pore network has radius of curvature r at the boundary and different curvatures (*e.g.*, r_{B1} and r_{B2}) inside each pore.

of fusion is not a strong function of temperature, we can approximate λ by:

$$\lambda\approx\frac{\Delta T_M}{\Delta T_F}=\frac{T_M(\infty)-T_M(r_B)}{T_M(\infty)-T_M(r_E)} \tag{10}$$

where ΔT_M is the undercooling where melting occurs in that pore and ΔT_F is the undercooling at which freezing occurs (*i.e.*, where the crystal/liquid interface enters the pore). In a cylindrical pore, where $r_E=r_B$, the entering ice has a hemispherical shape with a curvature of $2/(r_E-\delta)$; however, when that cylinder of ice melts, it has a curvature of $1/(r_E-\delta)$, so $\lambda=½$. For spheroidal pores (as in Fig. 5), λ is smaller, and can approach zero for a macroscopic pore with a mesoscopic entrance. The existence of the freezing/melting hysteresis can be seen in Fig. 8, since the measured contraction starts at about −2.7 °C on cooling and ends at about −1.3 °C on heating.

Thus, the pressure exerted by the crystal can be written in general as:

$$p_A = (1-\lambda)\int_T^{T_M(\infty)} \Delta S_{fv} dT \approx \Delta S_{fv}(\Delta T_F - \Delta T_M) \quad (11)$$

As the temperature continues to drop, the ice will propagate into smaller pores, as indicated in Fig. 5d. The radius of curvature at the leading edge of the ice is r, which decreases with temperature according to Eq. (6). Assuming that all of the pores remain in equilibrium, the pressure on the pore wall in each pore depends on the difference between the curvature of the pore body and that of the leading edge. That is, the pressure in each spherical pore is given by Eq. (8), with $\kappa_{CL}^S = 2/(r_B - \delta)$ and $\kappa_{CL}^E = 2/r$, where r is the radius of curvature in equilibrium at the current temperature according to Eq. (6). To find the net pressure exerted by the crystals, we need to take account of the volume fraction of pores of each size. If $\Phi_C(r_E)\, dr_E$ is the fraction of the pore space containing ice that has pore entry radius between r_E and $r_E + dr_E$, then the volume fraction of the pores that contain ice is:

$$\phi_C = \int_{r_{max}}^{r} \Phi_C(r_E) dr_E \quad (12)$$

where the integral is over the range of pore entry radii, from the largest, r_{max}, to the current size, $r(T)$; ϕ_C becomes equal to unity as r approaches the minimum pore entry size, r_{min}. For a body with polydisperse spheroidal pores, the term $\phi_C\, p_A$ in Eq. (3) should be replaced by:

$$\langle \phi_C p_A \rangle = \gamma_{CL} \int_{r_{max}}^{r} \left(\frac{2}{r} - \frac{2}{r_B - \delta} \right) \Phi_C(r_E) dr_E \quad (13)$$

or, using Eq. (6),

$$\langle \phi_C p_A \rangle = \phi_C \int_T^{T_M} \Delta S_{fv} dT - \int_{r_{max}}^{r} \left(\frac{2\gamma_{CL}}{r_B - \delta} \right) \Phi_C(r_E) dr_E \quad (14)$$

The pressure in the second integral in Eq. (14) can be written as:

$$\frac{2\gamma_{CL}}{r_B - \delta} = \int_{T_M(r_B)}^{T_M(\infty)} \Delta S_{fv} dT = \lambda \int_{T_M(r_E)}^{T_M(\infty)} \Delta S_{fv} dT \quad (15)$$

so the pressure can be expressed in terms of the undercooling:

$$\langle \phi_C p_A \rangle = \phi_C \int_T^{T_M} \Delta S_{fv} dT - \int_{r_{max}}^{r} \lambda \int_{T_M(r_E)}^{T_M(\infty)} \Delta S_{fv} dT \Phi_C(r_E) dr_E \quad (16)$$

To express the pressure without reference to pore radius, we can replace the pore size distribution with a melting point distribution:

$$\phi_C(T) = \int_T^{T_M(\infty)} \Phi_C\left(T'\right) dT' \quad (17)$$

where now $\Phi_C(T)\, dT$ is the fraction of the pore space accessible to ice at a temperature between T and $T + dT$. With this definition,

$$\langle \phi_C p_A \rangle = \phi_C \int_T^{T_M} \Delta S_{fv} dT - \int_T^{T_M(\infty)} \left(\lambda\left(T'\right) \int_{T'}^{T_M(\infty)} \Delta S_{fv} dT'' \right) \Phi_C\left(T'\right) dT' \quad (18)$$

From Eqs. (3), (7), and (18), the strain during freezing is found to be:

$$\varepsilon_x = \left(\frac{b}{3K_p} \right) \left\{ (2\phi_C - 1) \int_T^{T_M(\infty)} \Delta S_{fv} dT - \int_T^{T_M(\infty)} \left(\lambda\left(T'\right) \int_{T'}^{T_M(\infty)} \Delta S_{fv} dT'' \right) \Phi_C\left(T'\right) dT' \right\} + \int_{T_M(\infty)}^{T} \alpha dT \quad (19)$$

where b is the Biot coefficient [8], defined by:

$$b = 1 - \frac{K_p}{K_S} \approx \frac{2\phi}{1+\phi} \quad (20)$$

and the approximation follows from the Hashin–Shtrikman bound, Eq. (4). If the pores are monodisperse and uniform in shape, Eq. (19) reduces to:

$$\varepsilon_x \approx \left(\frac{b}{3K_p} \right) \Delta S_{fv}(T_M(\infty) - T)[(2-\lambda)\phi_C - 1] + \int_{T_M(\infty)}^{T} \alpha dT \quad (21)$$

According to Eq. (3), crystallization in air-entrained mortar causes contraction as long as $\phi_C p_A + (1-\phi_C) p_L < 0$ (that is, as long as the volume fraction of ice in the mesopores is small enough so that the crystallization pressure does not overwhelm the effect of the suction in the pore liquid. Using Eqs. (7) and (11), we find that (for pores of uniform size and shape) the positive pressure from the crystals dominates when $\phi_C(1-\lambda) > (1-\phi_C)$, so the critical fraction of ice beyond which the crystallization pressure exceeds the suction in the pore liquid is:

$$\phi_C^* > \frac{1}{2-\lambda} \quad (22)$$

Since $\lambda < 0.5$, the net pressure remains compressive until $\phi_C > 2/3$. (A more general condition is obtained by setting the expression in braces in Eq. (19) equal to zero.) This effect is offset by the thermal expansion coefficient of the mortar/ice composite, which increases with ϕ_C, augmenting the contraction during cooling. We can estimate the effect of ice on the thermal expansion coefficient of the mortar using the theory developed by Schapery [32] (see Appendix A); the result is shown in Fig. 1.

We can use the data in Fig. 1 to evaluate the parameter λ, as follows. The freezing curve (labeled ϕ_C, Freezing) indicates that the fraction of the pore space filled with ice reaches $\phi_C = 0.25$ when T drops to −13 °C, so $\Delta T_f = 13$; the melting curve (ϕ_C, Melting) indicates that this ice melts at −3.4 °C, so $\Delta T_m = 3.4$. According to Eq. (10), the shape factor for these pores is $\lambda \approx 3.4/13 = 0.26$. Based on the data in Brun et al. [15], the integral of the entropy (for pure water, in units of MPa/m^2) is

$$\int_T^{T_M} \Delta S_{fv} dT \approx -1.238T - 5.20 \times 10^{-3} T^2, \quad -40 \le T(^\circ C) \le 0 \quad (23)$$

A more precise estimate of λ can be obtained by using this result in Eq. (9). As shown in Fig. 6, the difference between the exact and approximate calculations is small, but the dependence on temperature is strong. At higher temperatures, where the volume of ice is small, the small value of λ indicates that the pores are spheroidal; as T

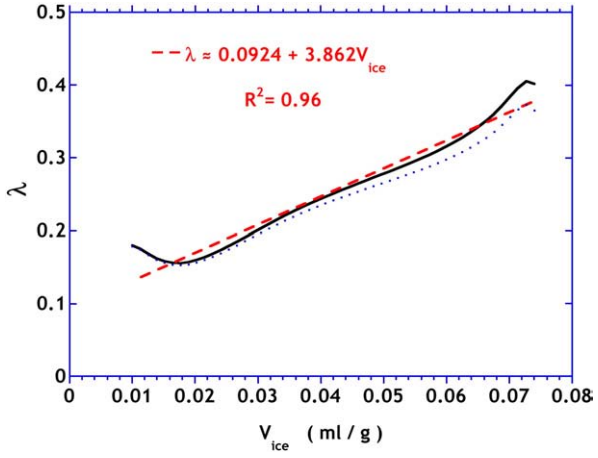

Fig. 6. The shape parameter, λ, calculated from the data in Fig. 1 using the exact expression, Eq. (9) (solid curve), and the approximation, Eq. (10) (dotted curve); also shown is a linear approximation to the exact result. Results are plotted as a function of the volume of ice per gram of solid matrix.

decreases, the ice enters smaller pores that are increasingly cylindrical in shape.

Now we have all the parameters needed to calculate the strain from Eq. (19). The components of the strain are shown separately in Fig. 7. The thermal expansion coefficient of the mortar alone, taken from Fig. 4, is $\alpha_S = -10.9\times10^{-6}°C^{-1}$. As ice forms, α increases considerably, as indicated in Fig. 1; integrating α over T leads to the thermal strain of Mortar + Ice shown in Fig. 7. The sum of the contributions from the pressure in the pore liquid and the crystallization pressure exerted by the ice is calculated from Eq. (19) with α set to zero. This pressure is negative, as long as the suction in the pore liquid has a greater effect than the positive crystallization pressure; in our mortars, the condition given in Eq. (22) is not reached at temperatures as low as −40 °C, so the net effect of crystallization remains compressive. All of the ice that is observed in the DSC is included in ϕ_C, so we are ignoring the ice that forms in the voids; that is, we are overestimating the positive pressure from ice in the mesopores. However, the ice in the voids will melt as the sample is heated above 0 °C, and the DSC results indicate that the amount of ice that melts at 0 °C is 1–4% of the total ice that forms; therefore, our approximate calculation is not seriously in error. The sum of all of these strains represents the total contraction of the body, which is compared in Fig. 8 to the strain measured in the DMA. The comparison is reasonably good, given the uncertainties in λ, α, and ϕ_C. Thus, the poromechanical computation can account quantitatively for the contraction observed in air-entrained samples, at least down to −25 °C.

The discrepancy between the measured and calculated strains is significant only below about −25 °C, where the measured strain begins to plateau, while the magnitude of the predicted strain continues to increase. This implies that there is another mechanism affecting the strain, such as formation of isolated pockets of water that burst when they freeze, or blockage of the surface pores on air voids that prevent the macroscopic ice from enhancing the suction in the pore liquid. It is also possible that this is the temperature at which the macroscopic ice is able to grow out of the voids into the mesopores, thus increasing the positive pressure on the solid phase; if so, it would imply that the pores in the shell of the air voids have radii of about 4 nm.

4.3. Scaling damage

According to the glue-spall theory [5], scaling damage happens when an ice layer on the surface of the concrete cracks, and the crack penetrates the surface. The stress that causes cracking results from the large difference in linear thermal expansion coefficient between ice (~$50\times10^{-6}°C^{-1}$ [33]) and concrete (~$10\times10^{-6}°C^{-1}$). As a salt solution freezes, the solute is not incorporated into the ice, but is rejected into the unfrozen brine; stress can only begin to build up after a continuous network of ice has developed. Valenza and Scherer [5,34] calculated the stress in the ice, based on data from the literature for elastic modulus and strength of frozen brine. We have recently discovered that some of those data were erroneous, because they reported concentrations as percent salt, when they were actually parts per thousand salt. The best available data for the flexural strength, σ_T, of frozen NaCl–water solutions, compiled by Timco and O'Brien [35–39], are presented in Fig. 9 as a function of the volume fraction of unfrozen brine, v_B. The scatter is quite large, but a reasonable approximation is given by:

$$\sigma_T(\text{MPa}) \approx 1.76\exp(-5.88\sqrt{v_B}) \tag{24}$$

The best available data for the static elastic modulus of these solutions are presented in Fig. 10 [37,40–44]. Again, the range of values is very broad, but a rough approximation is given by:

$$E(\text{GPa}) \approx 10\exp(-7.1\sqrt{v_B}) \tag{25}$$

As the temperature decreases, the stiffness of the frozen layer will increase, which will allow the thermal stress to rise. Cracking of the layer will occur when the stress exceeds its strength.

For the crack to penetrate the surface of the concrete, as in Fig. 11, the stress must satisfy a criterion developed by Thouless et al. [45].

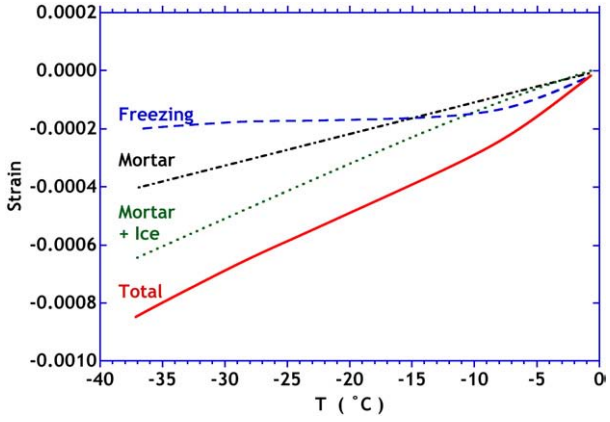

Fig. 7. Calculated strains during cooling cycle: Mortar = thermal strain of mortar ($\alpha_S = -10.6\times10^{-6}°C^{-1}$, from Fig. 4); Mortar + Ice = thermal strain of mortar containing ice, with α (from Fig. 1) calculated using composite theory from Ref. [32]; Freezing = strain from crystallization, from Eq. (19) with $\alpha = 0$; Total = sum of thermal and crystallization strains from Eq. (19).

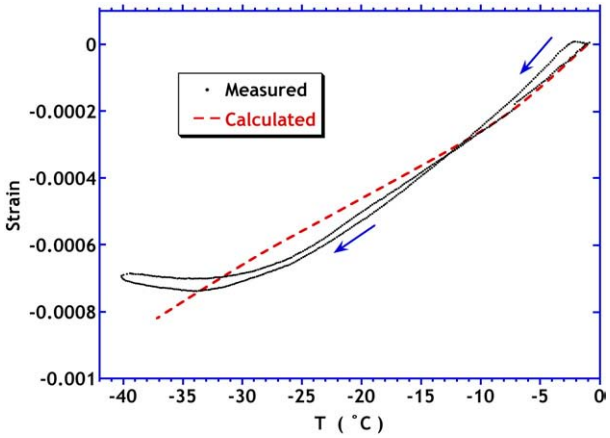

Fig. 8. Strain measured in DMA for mortar with 6% air (Measured) and strain (Calculated) from Eq. (19). Arrows indicate the direction of the temperature change.

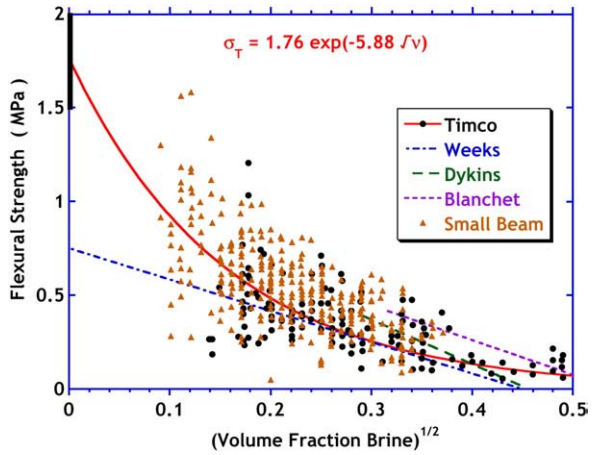

Fig. 9. Flexural strength of frozen solutions of NaCl in water, compiled by Timco and O'Brien [35].

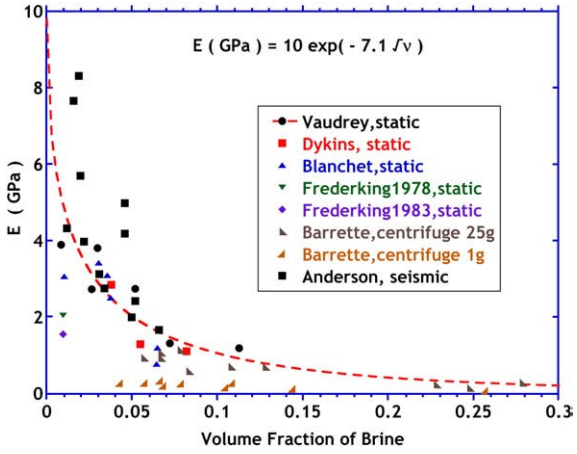

Fig. 10. Static elastic modulus of frozen solutions of NaCl in water. Data from Vaudrey [43, 44], Dykins [38,39], Blanchet et al. [37], Frederking and Timco [42], Barrette et al. [41], and Anderson [40].

When the concrete is much thicker than the ice layer, the criterion reduces to:

$$K_I \approx \frac{2.6\sigma_0 t_I}{\sqrt{\pi d_C}} \geq K_{Ic} \tag{26}$$

where K_I and K_{Ic} are the stress intensity and critical stress intensity of the surface of the concrete, respectively, t_I is the thickness of the ice, d_C is the depth of the crack in the concrete, and σ_0 is the thermal stress in the ice layer.[2] Since cracking of the ice requires that the thermal stress exceed the tensile strength, we conclude that a crack will penetrate the concrete surface when:

$$\sigma_0 > \sigma_T > \frac{0.68 K_{Ic}\sqrt{d_C}}{t_I} \tag{27}$$

The stresses presented in Fig. 12 were calculated by the method described in Ref. [34], except that the elastic moduli were taken from Eq. (25), and the thermal cycle was the one actually used in the experiments [6]. If the stress exceeds the strength from Eq. (24), it is assumed that cracks occur in the ice and that the stress drops to become equal to the strength. For the sample without air entrainment, this is predicted to occur at about −10 °C, when the strength is 0.11 MPa and the volume fraction of ice is about 0.78. For the samples with 3 or 6% air entrainment, owing to the contraction of the substrate caused by ice in the voids, the stress in the ice layer never exceeds the strength of the ice, so no scaling should occur in the air-entrained mortars. To predict the depth of penetration of a crack into the concrete substrate, we need a value for K_{Ic}. In Ref. [5], a value of 0.1 MPa·m$^{1/2}$ was adopted, as it is characteristic of the interfacial transition zone, and scaling cracks are reported to follow the interface around the aggregate [7,46]. Using that value, at the lowest temperature of the cycle (about −17 °C), Eq. (27) predicts that d_C would be about 0.1 mm for $t_I = 4$ mm, and 0.45 mm for $t_I = 8$ mm.

4.4. Nucleation and growth

Ice forms in porous materials by heterogeneous nucleation, and the temperature at which it forms depends on the contact angle between the ice and the nucleating substrate. As the size of the body decreases, the probability of finding a substrate with a low contact angle decreases, so ice forms at lower temperatures in smaller bodies. This is evident in comparing the temperature of freezing of −14.0 ± 0.4 °C in DSC samples (~0.05 g) with −10 to −12 °C in DMA samples (~0.7 g), and −3 to −5 °C in brick-size pieces (~465 g). What is particularly important in the present context is that the nucleation temperatures are the same in mortars with and without air entrainment, so there is no indication that nucleation is favored in the voids. How, then, does the ice get into the voids quickly enough to cause the immediate contraction seen in Fig. 2? Once ice nucleates, it can propagate through the mortar at a rate on the order of several mm/s [47]. Therefore, one might argue that the ice crystals penetrate into the voids as they pass through the paste. However, if they can grow through the pores in the shells surrounding the voids, they should be able to pass out through the shells, rather than exerting suction on the mesopores. More likely, the volume change that occurs as the ice grows through the paste causes a pressure wave that pushes water into the voids, where it immediately freezes. In fact, this phenomenon has been seen by Corr et al. [48]. Since the pressure wave runs ahead of the propagating ice, the ice might freeze in the voids before the neighboring mesopores begin to crystallize. That would mean that the contraction from the pore suction would quickly offset the crystallization pressure from the ice in the mesopores. Since the nucleation does not occur first in the voids, then crystallization pressure is exerted in the mesopores in every freezing cycle, before the contraction begins. This could lead to frost damage by fatigue over many freezing cycles. If so, then it might be beneficial to stimulate nucleation by including nucleating agents in the voids, so that ice forms there before it occurs spontaneously in the mesopores [49].

Based on the variation in freezing temperature with sample size in our samples, we estimate (see Appendix B) that there would be one nucleus capable of producing ice at −1 °C in a cube of mortar roughly 35 cm on an edge (~80 kg), or one per square meter in a plate 3 cm

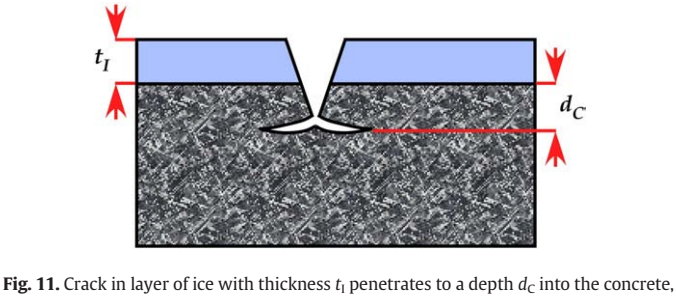

Fig. 11. Crack in layer of ice with thickness t_I penetrates to a depth d_C into the concrete, then bifurcates and runs parallel to the surface.

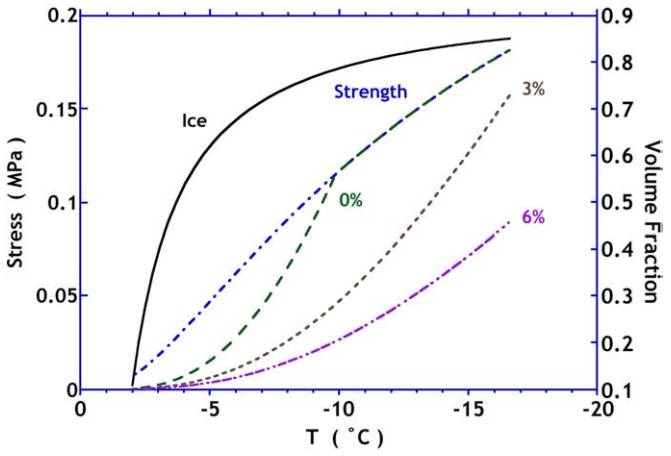

Fig. 12. Calculated stress in frozen brine layer containing 0, 3, or 6% air (indicated on curves); the curve labeled "Strength" is the flexural strength of the frozen brine, based on Eq. (24); the curve labeled "Ice" is the volume fraction of ice in the frozen brine, and refers to the right ordinate.

[2] This criterion was discussed in Ref. [5], but there was a typographical error in the definition of the parameter ω, which should have been (in the notation of that paper) $\omega = d/t_f - 1$.

thick. This may mean that the nature of freezing damage in the field is very different from that in the laboratory, because the large size of civil structures means that good nucleating agents are inevitably present. For example, on a road surface or sidewalk, we would estimate that one nucleus forms per square meter at about -1 °C, then the ice propagates through the pores as the temperature drops. This might avoid the shock of hydraulic pressure that occurs in a small lab sample (*e.g.*, Fig. 3) when nucleation occurs at a low temperature. However, even if ice nucleates near 0 °C, it cannot spread through a pore with radius r, until the temperature is low enough to satisfy Eq. (6). To spread arbitrarily far through the network of pores, the temperature has to reach the breakthrough point (see discussion of Fig. 5 in Ref. [27]), where the radius of the ice is small enough to enter a network of pores that percolates through the body. If we suppose that this point corresponds to the temperature where the intrusion increases rapidly during the freezing cycle in Fig. 1, then breakthrough only occurs at about $T_{BT}\approx$-7 °C ($r_{BT}\approx$10 nm). As the temperature drops toward that point in a large structure, nucleation might still occur in an isolated pocket of water at a substantial undercooling, resulting in a significant stress being suffered by the concrete. Unfortunately, there seems to have been no systematic investigation of nucleation in large concrete bodies.

Suppose that nucleation occurs at a temperature near zero, so that the ice penetrates progressively through the pores as the ambient temperature drops. In that case, the hydraulic pressure may be negligible, so one might ask whether air entrainment is necessary. We can calculate the strain that would result from the presence of ice crystals in mesopores, when the pore liquid remains at ambient pressure, by setting $p_L=0$ in Eq. (3). In the notation of Eq. (19), the strain from crystallization pressure is found to be:

$$\varepsilon_x^C\approx\left(\frac{b}{3K_p}\right)\langle\phi_C p_A\rangle=\left(\frac{b}{3K_p}\right)\left[\phi_C\int_T^{T_M}\Delta S_{fv}dT-\int_T^{T_M(\infty)}\left(\lambda\left(T'\right)\int_{T'}^{T_M(\infty)}\Delta S_{fv}dT''\right)\Phi_C\left(T'\right)dT'\right]$$
$$\approx\left(\frac{b}{3K_p}\right)\phi_C\Delta S_{fv}(T_M-T)(1-\lambda) \tag{28}$$

where the approximation applies for monodisperse pores of uniform shape. The rigorous result is shown in Fig. 13 (calculated using the properties of the mortar with 6% air). The dashed lines indicate the strain at which tensile failure is expected in this mortar (as estimated in Section 4.1). The crystallization pressure imposes a strain in excess of the tensile limit when T falls below about −34 °C. Thus, if the nucleation and growth process occurs slowly enough to avoid hydraulic pressure, then this mortar would not fail in a single freezing cycle, unless it was taken below −34 °C. Of course, failure could result from fatigue following many cycles that generate smaller strains. Alternatively, the damage seen in non-air-entrained mortars in cycles that only descend to −20 °C might result from pressure bursts when ice nucleates in isolated regions that exist above the breakthrough temperature. For example, in the present case, where $T_{BT}\approx-7$ °C, a nucleation event in the mesopores at −6 °C would cause a high localized pressure; in an air-entrained sample, that pressure would be over-balanced by the suction from ice in the voids.

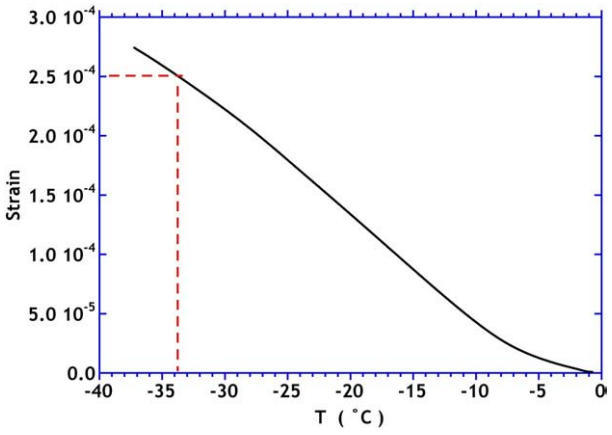

Fig. 13. Calculated strain in mortar without air entrainment, if crystallization is slow enough to avoid hydraulic pressure; calculated using the properties of the mortar with 6% air in Eq. (28). The dashed lines indicate the strain at which tensile failure is expected in this mortar.

5. Conclusions

In saturated laboratory samples without air entrainment, nucleation occurs at a low temperature, resulting in high hydraulic pressure and immediate damage. When air entrainment is present, nucleation occurs at the same low temperature, but the body contracts and there is no noticeable damage. Nevertheless, the evidence suggests that a significant amount of ice has to form in the mesopores to push water into the voids, which means that crystallization pressure is exerted during every freezing cycle. We have calculated macroscopic strains, which show an overall contraction of the air-entrained mortar throughout the freezing cycle; however, the local stresses around crystals in the mesopores may be tensile. This could lead to fatigue damage over many cycles, even when proper air entrainment is present.

Since the temperature of nucleation rises with the size of the sample, it is likely that ice forms at higher temperatures in the field, but the way ice propagates through a large structure, and the frequency of nucleation at low temperature in isolated regions are not known. Even when nucleation happens at small undercoolings, so that drastic hydraulic pressure does not occur, our calculations indicate that the crystallization pressure may exceed the tensile strength at low temperatures.

Once ice forms in the voids in air-entrained mortar or concrete, the ice creates suction in the surrounding mesopores. The body contracts by an amount that is quantitatively predicted by poromechanics. This contraction accounts for the protection of the body, as originally explained by Powers and Helmuth.

The contraction of air-entrained concrete also accounts for the beneficial effect of air entrainment on salt scaling. Calculations based on the glue-spall theory show that no scaling is expected in mortars with 3 or 6% air, whereas non-air-entrained samples are predicted to suffer damage. We conclude that the glue-spall theory successfully explains every experimental observation related to salt scaling.

Acknowledgments

This work was supported by NSF Grant CMS-0509986. The authors are indebted to Marie-Hélène Tremblay and Jacques Marchand for providing the mortar samples used in this work.

Appendix A. Thermal expansion coefficient of partially frozen mortar

Eq. (32) of the paper by Schapery [32] provides bounds on the thermal expansion coefficient of a multiphase material. In the present case, we are interested in a mortar whose pores contain a mixture of water and ice, so we have a three-phase composite. The water is assumed to be free to flow, so it does not exert pressure on the solid and therefore does not contribute to the expansion; that is, its bulk modulus is effectively zero. When ice forms in air voids, there is suction in the liquid that contributes to contraction of the body, but that is calculated separately; here we only consider thermal expansion effects. When the bulk modulus of one phase is zero, Schapery's bounds on the linear thermal expansion coefficient reduce

to:

$$\alpha = \frac{\langle K\alpha\rangle}{\langle K\rangle} \pm \left(\frac{1}{\tilde{K}} - \frac{1}{\langle K\rangle}\right)^{1/2}\left(\langle K\alpha^2\rangle - \frac{\langle K\alpha\rangle^2}{\langle K\rangle}\right)^{1/2} \tag{29}$$

where:

$$\langle K\alpha^m\rangle = \sum_{n=1}^{N} K_n \alpha_n^m v_n \tag{30}$$

and K_n, α_n, and v_n are the bulk modulus, thermal expansion coefficient, and volume fraction of phase n in a composite of N phases. The quantity $\tilde{K}$ in Eq. (29) is the bulk modulus of the composite, which can be estimated from the Hashin–Shtrikman bounds. The lowest upper bound on K for a three-phase composite consisting of water ($E=0$), ice ($E=10$ GPa, $\nu=0.33$ [33,50], $K=8.3$ GPa), and mortar ($E_S=32.0$ GPa, $\nu_S=0.2$, $K_S=17.8$ GPa), is given by the Hashin and Shtrikman theory as:

$$K_{LU} = \frac{17.78(1-v_w)-6.43v_{ice}}{1+v_w+v_{ice}} \tag{31}$$

where $v_w=\phi\,(1-\phi_C)$ is the volume fraction of water and $v_{ice}=\phi\,\phi_C$ is the volume fraction of ice.

Inserting the property values for the phases and plotting Eq. (29), we find that the appropriate bound corresponds to the positive sign in that equation. The result is shown in Fig. 1. The lower bound, given by the negative sign in Eq. (29), shows a non-monotonic dependence of α on the volume fraction of ice.

Appendix B. Frequency of nucleation in a porous body

Suppose that the cooling rate is $q=dT/dt$ (°C/s) and the interval of observation is $\Delta t=\Delta T/q$. To see a nucleation event in a porous body with volume V, the nucleation rate, I_v ($cm^{-3}s^{-1}$), has to satisfy the following condition:

$$I_v V\Delta T/q \geq 1 \tag{32}$$

Suppose that the total surface area in contact with the liquid per unit volume of the body is A and that the fraction $h(\theta)$ of the surface has heterogeneous nucleation sites with contact angle θ. Let it be a discrete distribution of contact angles, θ_n, and let $h_n=h(\theta_n)$, so that:

$$\sum_{n=1}^{N} h_n = 1 \tag{33}$$

If the specific surface area of the solid phase is s_{BET} (m^2/kg) and the bulk density is ρ_b (kg/m^3), then $A=\rho_b\, s_{BET}$. The heterogeneous nucleation rate attributable to each quality of substrate [51] is:

$$I_v^n = h_n \rho_b s_{BET}\left(\frac{N_A kT}{3\pi\Omega\eta}\right)\exp\left(-\frac{\Delta G_{hom} f(\theta_n)}{kT}\right) \tag{34}$$

where Ω is the molecular volume, $N_A \approx 1/\Omega^{2/3}$ is the number of liquid molecules per unit area, and η is the viscosity of the liquid. The total nucleation rate is:

$$I_v = \sum_{n=1}^{N} I_v^n \tag{35}$$

For a spherical nucleus [51],

$$\Delta G_{hom} = \frac{16\pi\gamma_{CL}^3}{3(T_M-T)^2\Delta S_{fv}^2} \tag{36}$$

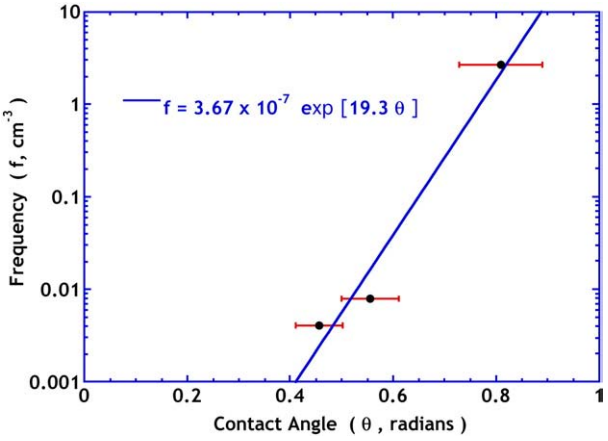

Fig. 14. Number of sites per cm^3 with contact angle θ calculated from Eq. (38), based on nucleation temperatures observed in mortar samples with sizes between 0.4 and 250 cm^3.

and for a spherical cap on the substrate,

$$f(\theta) = \frac{1}{4}[2-3\cos(\theta)+\cos^3(\theta)] \tag{37}$$

Generalizing Eq. (32), a crystal is observed when:

$$1 = V\int_0^t I_v dt = V\int_{T_0}^{T}(I_v/q)dT \tag{38}$$

Evaluating this expression using handbook values for the properties of water, we find that the result is very weakly dependent on V, q, or h_n, but is strongly dependent on the contact angle, θ. That is, for the range of sample sizes used in this study (~0.4–250 cm^3), and for cooling rates between 1 °C/min and 1 °C/h, the temperature of nucleation only varies by a few tenths of a degree for a given contact angle. Therefore, we can construct an approximate curve relating the nucleation temperature to θ. We can also find the contact angle that would yield nucleation at a certain temperature in a given volume of material. Using the sample sizes and nucleation temperatures observed in our experiments, we obtain the result shown in Fig. 14. These very preliminary data indicate that the frequency (number/cm^3) is:

$$F(\theta) = 3.67\times 10^{-7}\exp(19.3\theta) \tag{39}$$

To obtain nucleation at −1 °C would require a site with $\theta\approx 0.22$ radians. Extrapolating Eq. (39), we find that there should be one such site in 39,000 cm^3, or a cube 34 cm on an edge. Of course, this is a crude estimate based on only a few measurements. Far more data are needed for the nucleation temperature versus sample size for a range of cementitious materials, so that the field behavior can be reliably predicted.

References

[1] G.J. Verbeck, P. Klieger, Studies of "salt" scaling of concrete, Highw. Res. Board Bull. 150 (1957) 1–17.
[2] J. Marchand, R. Pleau, R. Gagné, Deterioration of concrete due to freezing and thawing, in: J. Skalny, S. Mindess (Eds.), Materials Science of Concrete IV, Am. Ceram. Soc., Westerville, OH, 1995, pp. 283–354.
[3] J.J. Valenza II, G.W. Scherer, A review of salt scaling: I. Phenomenology, Cem. Concr. Res. 37 (2007) 1007–1021.
[4] J.J. Valenza II, G.W. Scherer, A review of salt scaling: II. Mechanisms, Cem. Concr. Res. 37 (2007) 1022–1034.
[5] J.J. Valenza II, G.W. Scherer, Mechanism for salt scaling, J. Am. Ceram. Soc. 89 (4) (2006) 1161–1179.
[6] M.-H. Tremblay, F. Lory, J. Marchand, G.W. Scherer, J.J. Valenza, Ability of the glue spall model to account for the de-icer salt scaling deterioration of concrete, in: J.J. Beaudoin, J.M. Makar, L. Raki (Eds.), paper W4-07.3 in Proc. 12th ICCC, National Research Council of Canada, Montreal, Canada, 2007, ISBN 978-0-660-19695-4.

[7] O. Çopuroğlu, E. Schlangen, Modeling of frost salt scaling, Cem. Concr. Res. 38 (2008) 27–39.
[8] O. Coussy, Poromechanics, Wiley, West Sussex, England, 2004.
[9] O. Coussy, P.J.M. Monteiro, Poroelastic model for concrete exposed to freezing temperatures, Cem. Concr. Res. 38 (2008) 40–48.
[10] Z. Sun, G.W. Scherer, "Pore size and shape in mortar", submitted to Cement Concr. Res.
[11] N. Fukuta, Ice nucleation by metaldehyde, Nature 199 (1963) 475–476.
[12] R.F. Feldman, in: L.R. Roberts, J.P. Skalny (Eds.), The porosity and pore structure of hydrated Portland cement paste, Pore Structure and Permeability of Cementitious Materials, vol. 137, Materials Research Society, Pittsburgh, PA, 1989, pp. 59–73.
[13] N.C. Collier, J.H. Sharp, N.B. Milestone, J. Hill, I.H. Godfrey, The influence of water removal techniques on the composition and microstructure of hardened cement pastes, Cem. Concr. Res. 38 (2008) 737–744.
[14] S. Ghabezloo, J. Sulem, S. Guédon, F. Martineau, J. Saint-Marc, Poromechanical behaviour of hardened cement paste under isotropic loading, Cement Concr. Res. 38 (12) (2008) 1424–1437.
[15] M. Brun, A. Lallemand, J.F. Quinson, C. Eyraud, A new method for the simultaneous determination of the size and the shape of pores: the thermoporometry, Thermochim. Acta 21 (1977) 59–88.
[16] G.W. Scherer, D.M. Smith, D. Stein, Deformation of aerogels during characterization, J. Non-Cryst. Solids 186 (1995) 309–315.
[17] J. Villadsen, Pore structure in cement based materials, Tech. Rep., vol. 277, Building Materials Lab., Technical Univ, Denmark, 1992, ISSN 0908-3871.
[18] G.W. Scherer, J.J. Valenza II, G. Simmons, New methods to measure liquid permeability in porous materials, Cem. Concr. Res. 37 (2007) 386–397.
[19] T.C. Powers, L.E. Copeland, J.C. Hayes, H.M. Mann, Permeability of Portland cement paste, Bull. Portland Cem. Assoc. 53 (1955) 285–298.
[20] R.A. Olson, C.M. Neubauer, H.M. Jennings, Damage to the pore structure of hardened Portland cement paste by mercury intrusion, J. Am. Ceram. Soc. 80 (9) (1997) 2454–2458.
[21] T.C. Powers, R.A. Helmuth, Theory of volume changes in hardened Portland-cement paste during freezing, Proc. Highw. Res. Board 32 (1953) 285–297.
[22] O. Coussy, P.J.M. Monteiro, "Errata to "Poroelastic model for concrete exposed to freezing temperatures" [Cement and Concrete Research 38 (2008) 40–48]", Cement and Concrete Research 39 (2009) 371–372
[23] R.C. Weast, M.J. Astle (Eds.), CRC Handbook of Chemistry and Physics, 62nd ed, CRC Press, Boca Raton, FL, 1981.
[24] V.R. Parameswaran, Orientation dependence of elastic constants for ice, Def. Sci. J. 37 (3) (1987) 367–375.
[25] W. Vichit-Vadakan, G.W. Scherer, "Measuring permeability of rigid materials by a beam-bending method: III. Cement paste", J. Am. Ceram. Soc. 85 (6) 1537–44 (2002); Erratum, J. Am. Ceram. Soc. 87 (8) (2004) 1615.
[26] Z. Hashin, S. Shtrikman, A variational approach to the theory of the elastic behavior of multiphase materials, J. Mech. Phys. Solids 11 (1963) 127–140.
[27] G.W. Scherer, J.J. Valenza II, Mechanisms of frost damage, in: J. Skalny, F. Young (Eds.), Materials Science of Concrete, Am. Ceram. Soc., vol. VII, 2005, pp. 209–246.
[28] J.M. Lee, Y. Soong, Effects of surfactants on the liquid–liquid dispersions in agitated vessels, Ind. Eng. Chem. Process Des. Dev. 24 (1985) 118–121.
[29] M.H. Schroth, J.D. Istok, S.J. Ahearn, J.S. Selker, Geometry and position of light nonaqueous-phase liquid lenses in water-wetted porous media, J. Contam. Hydrol. 19 (1995) 269–287.
[30] H. Teng, C.M. Kinoshita, S.M. Masutani, Prediction of droplet size from the breakup of cylindrical liquid jets, Int. J. Multiph. Flow 21 (I) (1995) 129–136.
[31] G.W. Scherer, Stress from crystallization of salt, Cem. Concr. Res. 34 (2004) 1613–1624.
[32] R.A. Schapery, Thermal expansion coefficients of composite materials based on energy principles, J. Compos. Mater. 2 (1968) 380–404.
[33] E.R. Pounder, Physics of Ice, Pergamon Press, Oxford, 1965.
[34] J.J. Valenza II, G.W. Scherer, Mechanism for salt scaling of a cementitious surface, Mater. Struct. 40 (2007) 259–268.
[35] G.W. Timco, S. O'Brien, Flexural strength equation for sea ice, Cold Reg. Sci. Technol. 22 (1994) 285–298.
[36] W. Weeks, D. Anderson, An experimental study of strength of young sea ice, Trans. Am. Geophys. Union 4 (4) (1958) 641–647.
[37] D. Blanchet, R. Abdelnour, G. Comfort, Mechanical properties of first-year sea ice at Tarsiut Island, J. Cold Reg. Eng. 11 (1) (March, 1997) 59–83.
[38] J.E. Dykins, Ice engineering: material properties of saline ice for a limited range of conditions, Technical Report R720, US Naval Civil Eng. Lab, Port Hueneme, California, 1971.
[39] J.E. Dykins, Tensile and flexural properties of saline ice, in: N. Riehl, B. Bullemer, H. Engelhardt (Eds.), Physics of Ice, Plenum Press, New York, NY, 1968, pp. 251–270.
[40] D.L. Anderson, Preliminary results and review of sea ice elasticity and related studies, Trans. Eng. Inst. Can. 2 (1958) 116–122.
[41] P.D. Barrette, R. Phillips, J.I. Clark, G. Crocker, S.J. Jones, Flexural behavior of model sea ice in a centrifuge, J. Cold Reg. Eng. 13 (3) (Sep, 1999) 122–138.
[42] R.M.W. Frederking, G.W. Timco, On measuring flexural properties of ice using cantilever beams, Ann. Glaciol. 4 (1983) 58–65.
[43] K.D. Vaudrey, Ice engineering—study of related properties of floating sea-ice sheets and summary of elastic and viscoelastic analyses, Technical Report R860, US Navy Civil Engineering Laboratory, Port Hueneme, California, 1977.
[44] K.D. Vaudrey, Determination of mechanical sea ice properties by large scale field beam experiments, in: D.B. Muggeridge (Ed.), POAC '77-Fourth Int. Conf. Port and Ocean Engineering Under Arctic Conditions, vol. I, Ocean Engineering Information Center, Memorial University of Newfoundland, St. John's, Canada, 1977, pp. 529–543.
[45] M.D. Thouless, A.G. Evans, M.F. Ashby, J.W. Hutchinson, The edge cracking and spalling of brittle plates, Acta Metall. 35 (6) (1987) 1333–1341.
[46] D. Jana, Concrete construction or salt—which causes scaling? Concr. Int. 26 (11) (2004) 31–38.
[47] Z. Sun, D. Kumpf, G.W. Scherer, Kinetics of ice growth in concrete, in: J.J. Beaudoin, J.M. Makar, L. Raki (Eds.), paper W4-07.1 in Proc. 12th Int. Cong. Cement Chemistry, National Research Council of Canada, Montreal, Canada, 2007, ISBN 978-0-660-19695-4.
[48] D.J. Corr, P.J.M. Monteiro, J. Bastacky, "Microscopic characterization of ice morphology in entrained air voids", ACI Mater. J. 99-M18 [March–April] (2002) 190–195.
[49] G.W. Scherer, J. Chen, J. Valenza, "Method of protecting concrete from freeze damage", U.S. Pat 6, 485, 560 (Nov. 26, 2002).
[50] R.E. Gagnon, S.J. Jones, Elastic properties of ice, Ch. 9, in: Levy, Bass, Stern (Eds.), Handbook of Elastic Properties of Solids, Liquids, and Gases, Elastic Properties of Solids: Biological and Organic Materials, vol. III, Academic, New York, 2001, pp. 229–257.
[51] J.W. Christian, The Theory of Transformations in Metals and Alloys, Part I, Pergamon, New York, 1975.